coatings

MDPI

Article

Modeling the Shape and Clarifying the Condition of a Moving S-N Border During Pulsed S-N Switching of YBCO Thin Films

Oleg Kiprijanovič * and Linas Ardaravičius

Center for Physical Sciences and Technology, Saulėtekio al. 3, LT-10257 Vilnius, Lithuania; linas.ardaravicius@ftmc.lt
* Correspondence: oleg.kiprijanovic@ftmc.lt

Highlights

- Moving S-N border continuously and randomly changes its shape, with the emergence of fractal-like structures.
- Reconnecting of the border S currentsinduces enclosed microscopic S areas with quantum properties.
- Moving S-N border is constantly being in unstable state resembling MHD Richtmyer–Meshkov instability.

Abstract

Transition from the superconducting (S) to the normal (N) state in YBCO thin films (S-N switching) induced by nanosecond current pulses has been studied extensively. Still, the properties of the moving S-N border during N zone propagation have not yet been identified. This paper continues a theoretical and descriptive study aimed at modeling the real shape and condition of the moving border. The bent shape of the border is caused by the opposition between the Meissner and Lorentz forces. The equilibrium of these forces leads to bifurcations and the buckling of valleys. To better understand the dynamic changes in the border, we present two additional local propagation developments preceded by bifurcation and subsequent reconnection of the border's S currents. The incompressibility of the Meissner currents intricately alters the border's shape. Its other properties such as extreme flexibility and high tensile strength allow us to present its quasi-real fractalized form. The phase transition and the heat replenishing the energy loss ahead of the border indicate ultrafast N zone propagation exhibiting combustion wave properties. The discussion substantiates that during propagation, the S-N border is in a condition of constantly being in an unstable state, resembling a magnetohydrodynamic (MHD) Richtmyer–Meshkov instability.

Keywords: YBCO thin films; pulsed S-N switching; microscopic S areas; MHD bending instability; MHD Richtmyer–Meshkov instability

Check for updates

Academic Editor: Shuai Chen

Received: 25 September 2026
Revised: 29 October 2026
Accepted: 30 October 2026
Published: 1 November 2026

Copyright: © 2026 by the authors. Licensee MDPI, Basel, Switzerland. This article is an open access article distributed under the terms and conditions of the Creative Commons Attribution (CC BY) license.

1. Introduction

High-temperature superconductors discovered in 1986 turned out to be type II superconductors. Due to the unique properties of the border between superconducting (S) and normal (N) state (S-N border), they allow the penetration of the magnetic field by magnetic flux quanta (Abrikosov vortices), so-called incomplete Meissner effect [1,2]. External magnetic flux, trapped in a closed area of the type-II superconductor, always has an integer number of vortices. This, along with the 2*e* charge in fundamental formulas, indicates

not only the quantum nature of the S state, but also its collective quantum interaction in a Bose condensate of Cooper pairs: macroscopic collective quantum state (MCQS) [3]. Recently, scientists researching MCQSs have been encouraged by the possibility of quantum effects manifesting not only in the elementary components of an MCQS but also within its macroscopic volumes [4,5]. Although the boom in superconductivity research subsided after 2000, studies, including investigations into thin films, continue [6].

Experiments conducted by irradiating the S films with short optical pulses have shown that the S state initially withdraws its S-N border from the irradiated area at the Fermi velocity [7,8]. This suggests the possibility of creating ultrafast switches by applying short optical, current, or magnetic pulses to the films, thereby, implementing a fast transition from the S to the N state (S-N switching).

Significant information on the S-N border shape changing during N zone propagation was obtained by studying scanning electron microscope (SEM) images of films damaged by overcritical, fast-rising, short electrical pulses [9]. Some difficulties in achieving ultra-fast switching velocities were identified. Based on the obtained information, a model founded on idealized stepwise N zone propagation was proposed [10]. This model assumes an inhomogeneous current distribution with a high-density S current "thread" of λ_{eff} thickness at the YBCO film edges [11] and presents the N zone propagation without any film damage. According to this model, the beginning of the S-N switching is driven by the development of the magnetohydrodynamic (MHD) bending instability of this "thread". An unstable state arises in a 50–80 μm wide section on the opposite sides of the film due to the counteraction of the Meissner force to the Lorentz force on the S-N border during the fast pulse growth. Experiments show the formation of a primary N zone strip across the film as the unstable areas meet at the film's center. The current "thread" is considered a certain separate object having such properties as a very high tensile strength and extreme flexibility [10].

The buckling of valleys in the developed unstable state at one of the steps can be accompanied by the cumulative penetration of magnetic flux into the film, thereby penetrating the S state. The emergence of coherent jets containing a magnetic field during the buckling of the valleys occurs due to the incompressibility of the Meissner currents in the "thread" [12].

This MHD instability has an analog in mechanics, known as the Ishlinsky–Lavrent'ev instability [13]. In that scenario, a strong, sudden impact strikes a vertical rod, and its support acts as a counterforce. The rod is distorted into a wave-like shape. In our case, the rapidly increasing Lorentz force is applied perpendicularly to the "thread" and counteracted by the Meissner force, leading to wave-like bending, albeit on a microscopic scale.

During the non-damaging N zone propagation, the shape changes of the S-N border cannot be observed without an intricate technical arrangement, including a microscope coupled with a high-speed camera. While the damage by cumulative jets and the round dark spots, left by magnetic cumulation, are visible in the SEM images, other damage features can be identified partly. Therefore, the changes in the shape of the border over time cannot be reconstructed from images of the damaged films. We note that fast phenomena such as the cumulative buckling and the magnetic cumulation are accompanied by ultrashort pulses of electromagnetic radiation. The ultrashort time scales of these events indicate that the generated pulses are in the THz range, which is supported by preliminary theoretical estimates. To register such pulsed signals, sensitive S films were a suitable choice for the detectors [14,15]. Modern THz sensors using metamaterials are also currently emerging, offering an alternative approach to THz sensing alongside superconducting bolometers. One proposed and modeled example is a dual-band sensor based on an aluminum-silicon metamaterial with a central relief to enhance its sensitivity [16].

After 2010, the scientific community significantly shifted its attention to graphene due to its high charge carrier mobility and broadband optical response. Since then, graphene films have been used for sensitive detection in the THz range [17,18]. In particular, to reliably detect picosecond duration pulses, recent studies have proposed integrating a field-effect transistor with an epitaxial graphene channel with an asymmetric double-gating structure, which increases the sensitivity of the device [19]. Technologies associated with dual-function THz metamaterial absorbers based on microfluidic structures and uncooled infrared microbolometer materials are also advancing [20,21].

Modern fabrication technologies continue to enable the production of superconducting films suitable for experiments on pulsed S-N switching. Complementary investigations of irradiated S tapes encompass their microstructural, structural, magnetic, and electrical properties, elucidating the microscopic origins of irradiation-induced degradation [22].

The aim of the work is to model the instantaneous, quasi-realistic shape of the S-N border as the N zone propagates along a narrow channel across the film. Since the phase transition occurs as the unstable and wave-shaped S-N border moves, characterizing its condition remains an open challenge.

2. Bifurcation Behavior near the Equilibrium Points and S Currents Reconnections at the S-N Border

In the model presented in [10], an idealized S-N switching was considered for three qualitatively different YBCO films. It was described as a kind of cumulative step-by-step propagation of the N zone, in which the bulges of the wave-like S-N border become valleys, and then the valleys, conversely, become bulges. This is similar to a π-phase shift at each step.

The cumulative character of the ideal S-N border movement in ref [10] is insufficient to understand the changes which are inherent to the real border's shape. In addition to this idealized shape, we add two new elements of instability development during N zone propagation. These elements are reconstructed from indirect signs in the SEM images, with the interpretation guided by MHD laws and phenomena [23]. The first element was identified as a commonly encountered doubling bifurcation. The second was identified as a blocking of coherent jet penetration, an MHD phenomenon that occurs in plasma physics and superconductors. Developing instability reaches a state when the Meissner force counterbalances the Lorentz force at the tops of bulges which become bifurcation points. The S-N border shape changings as result of the bifurcation cause subsequent reconnections of the border's S current. The notation and classification of the thin YBCO films by quality are retained as in reference [10].

In the real movement of the S-N border, various bifurcation situations arise at different points along it. The prevalent bifurcation is the one that causes the bulge doubling. Instability development at one of the steps halts when the Meissner and Lorentz forces at the bulge tops are counterbalanced. Most probably, the bulge doubling is caused by the fact that the longitudinal component of the Lorentz force on the sides of the bulge begins to prevail over the longitudinal component of the Meissner force. The converging right- and left-hand branches of the adjacent split bulges extend the S-N border, which is energetically inefficient for the MCQS. This doubling bifurcation of bulge is most frequent in the films with λ_{eff} of about 2–3.5 μm width, meaning not sufficiently high critical current density. The stages of such an event are shown in Figure 1a,b.

As a result of the bifurcation at the equilibrium point, bulge doubling begins. Shown in Figure 1a is the rare case where the doubling occurs at every bulge. Subsequently, the right- and left-hand adjacent branches approach and converge at points m and n.

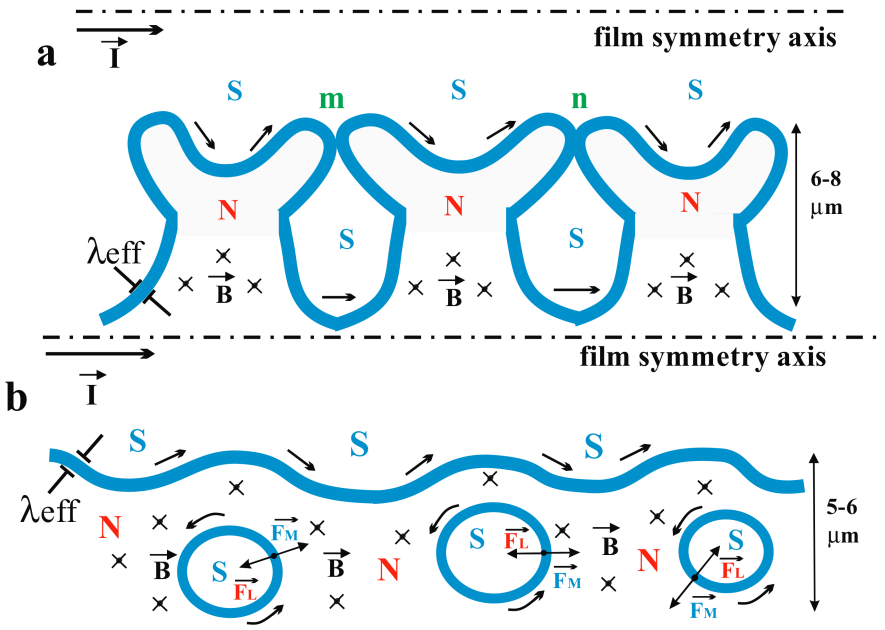


Figure 1. (**a**,**b**). Decay of a developed unstable state in the ideal case of the bulge doubling bifurcation. (**a**) Energetically inefficient stretching of the S-N border due to the convergence of the right- and left-hand branches. Currents reconnect at points **m** and **n**. Small arrows indicate the local S current direction. (**b**) Smoothed out S-N border after the current reconnection. Closed areas with minimal trapped magnetic flux surrounded by the N zone appear. Small arrows indicate the local S current direction. Top view.

For the S state, as an MCQS, maintaining the border with elongated drop-like regions becomes energetically inefficient. Consequently, the MCQS tends to minimize its length through reconnection, which occurs almost instantly at the points m and n. As a result, the enclosed S areas are surrounded by the N zone and falling under the influence of the expelled magnetic field (see Figure 1b). These areas contain minimal trapped magnetic flux, and their circular currents flow in direction that compensate for the external magnetic field, conserving the flux. This compensation is sustained by an increase in the circular S currents. These closed S areas rapidly shrink and disappear driven either by the circular S current reaching its critical value or simply by the prevalence of the Lorentz force. Once the S-N border becomes smoother following reconnection, the next step of the instability begins to develop. This process of the vanishing converts less energy into heat compared to magnetic cumulation.

The MCQS also exhibits its properties that weaken coherent jet action in the films having λ_{eff} of about 1.5–2 μm width, meaning that the film critical current density is higher than for the first element. In this case, due to another bifurcation, buckling of the valleys becomes prevalent, resulting in coherent jet formation. The blocking of the jet's penetrating action becomes very probable. If buckling occurs when the valley angle 2α exceeds π/4, the coherent jet will not have sufficient velocity to overcome the significant resistance of the Meissner force. As demonstrated in paper [8], the MCQS responds almost instantly to maintain its borders. Let us consider this process for a single valley, as illustrated in Figure 2a,b. Following buckling, the S-N border from both sides converges towards point O (see Figure 2a). Simultaneously the jet tip also penetrates to the point O. The MCQS blocks the penetrating action of the jet by reconnecting the S currents at point O. Unable to proceed, the jet is dispersed. As seen in Figure 2b, two closed microscopic S areas form after this reconnection. Like all closed S areas, they contain an integer number of magnetic flux quanta, also known as vortices. Density of the vortices in the S areas is low.

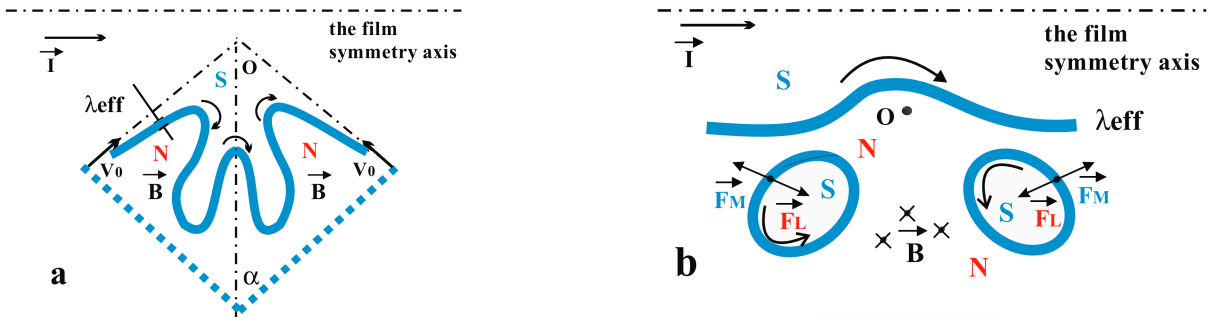


Figure 2. (**a**,**b**). Blocking of the penetrating action of a coherent jet by the S state acting as the MCQS. (**a**) Formation of a coherent jet and the reaction of the MCQS to prevent jet penetration. (**b**) Appearance of vanishing, microscopic S areas following the reconnection of the S currents at point **O**. Top view.

The calculation shows that, in this case, the jet velocity is equal to $V_0/\sin\alpha$. This is very close to the value of $(1/2)V_0\ \mathrm{ctg}(\alpha/2)$, and the coefficient 1/2, according to the hydrodynamic theory of the cumulative effect, indicates that the jet medium is as dense as the medium it penetrates into. And this is the result of the counteraction of the Meissner force.

3. Uncovering the Quasi-Real Shape of the Moving S-N Border

Now that the cumulative propagation is supplemented by the doubling of the bulge tops and incomplete cumulative penetration, the real shape of the S-N border becomes clearer. With each passing moment, the bifurcation points and the buckling of the valleys unpredictably change the shape of the S-N border. The changes will no longer be synchronized as in the idealized stepwise cases [10]. Therefore, at any moment, the S-N border will be shaped as an irregular wave-like curve. Yet one more factor must be considered. The extraordinary flexibility and high tensile strength of this current "thread" have already been mentioned. These properties lead to the appearance of smaller bent elements, indicating the emergence of fractality. Thus, the real shape of the S-N border combines two contradictory factors: while various bifurcations lead to its randomly perturbed shape, unique "thread" properties facilitate the appearance of certain fractalized structures.

The Lorentz force is perpendicular to the local current direction; therefore, the expansion of the N zone causes a change in the S current direction, which in turn alters the direction of the N zone's expansion. Such fast chaotic wave-like changes in the shape obscure and complicate the characterization of the S-N border condition during the N zone propagation. The unstable wave-like shape of the current "thread" promotes energy dissipation. Continuous changes facilitate partial S current energy conversion into heat, inducing the phase transition. Due to this, the edge of the N zone is constantly heated up, thus forcing a retreat of the S state. The phase transition and the support of the propagation by the release of the Joule heat indicate directly that, during non-destructive S-N switching, the N zone propagates as a fast-moving wave with the properties of a combustion wave [24]. Based on an analysis of factual conditions, Figure 3 presents the modeled quasi-real instantaneous shape of the S-N border. It is represented as a continuous curve because the reconnections occur almost instantaneously. The quasi-real shape shown in Figure 3 corresponds to the high-quality YBCO film with λ_{eff} width of 1–1.4 μm, meaning the highest critical current density. For the films with a wider λ_{eff}, there will be fewer bends, and the S-N border will be more diffuse during the propagation.

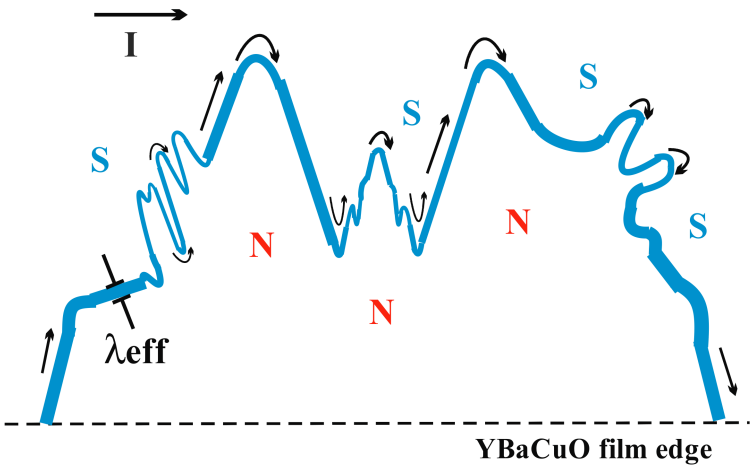


Figure 3. Quasi-real instantaneous shape of the moving S-N border constructed from factual conditions. Small arrows indicate the direction of the local S current. Top view.

4. Discussion

Having analyzed the influence of bifurcations on the shape of the S-N border, we can now proceed to search for a possible mathematical description of its modeled shape. The doubling dynamics for a subcritical pitchfork bifurcation can be modeled by solving an equation that incorporates a single variable parameter [25]. In the case of the buckling, a folded catastrophe surface, which depends on two variable parameters, is used to solve buckling problems in mechanics [26]. To model this propagation of the N zone, we should assign the "mechanical" characteristics to the S-N border. However, these properties will differ significantly from those of known mechanical objects and are currently unknown in quantitative terms. In addition to these "mechanical" properties, one should somehow determine both the S current density and the magnetic field induction at the exact moment of the developed instability decay. At this stage of decay, the current and the magnetic field become concentrated at the bulge tops and dispersed at the bottoms of the valleys.

The MQCS strictly maintains the integrity of its border, so we assume that reconnection of S currents occurs several orders of magnitude faster than changes in the shape during the propagation. The vanishing microscopic S areas contain an integer number of magnetic flux quanta and extending their lifetime sufficiently for practical use is currently not feasible. As the N zone propagates, bifurcation situations may occur at any point of the curved S-N border. The bifurcation outcome is characterized by the fact that the dynamics of change cannot be predicted. For example, the doubling bifurcation at the top of the bulge, depending on the local current distribution, may generate soft coherent jet instead of smooth reconnecting with the adjacent branches.

It is impossible to define an analytical formula for such a shape. Attention was turned to the Weierstrass function, which is defined as an infinite sum with certain parameters, that exhibit fractality [27]. However, its application fails due to the absence of random perturbations. In [28], some graphical shapes defined as m-th order prefractals of the Weierstrass function were proposed. In modeling the quasi-real shape shown in Figure 3, parts of the first-, second-, and third-order prefractals were combined with a corresponding increase in the number of sawteeth. However, any sharp angles must be rounded off, as the real S-N border shape cannot have them.

At each instant, the S-N border will be an irregular wave curve having a wide spectrum of harmonics. This border shape is typical of a boundary between two fluids of different densities, distorted by a passing shock wave, as would be the result of the Richtmyer–Meshkov instability [29]. In experiments to enhance the effect of the shock wave, this boundary

is sinusoidally perturbed before the wave arrives [30]. Recently, advances in computing technology and software have led to intensive studies of the MHD Richtmyer–Meshkov instability. The influence of a magnetic field on its development has been established [31–34].

Due to the presence of a magnetic field such instability is acceptable in our case. By definition, the Richtmyer–Meshkov instability requires a single passage of a shock wave through an interface or a thin layer. In our case the N zone propagates with a velocity which is higher than the shock wave velocity in solids. Thus, at any given moment, the moving S-N border has a shape with characteristic features of a boundary resulting from the passage of a shock wave through a thin layer in a magnetic field. Considering the phase transition and the support of the fast propagation by the release of Joule heat, the moving S-N border can be characterized as being constantly in a state of MHD Richtmyer–Meshkov instability.

Unexpectedly, new technologies open the way to study into the phenomena arising from the opposition of Meissner and Lorentz forces during the N zone propagation. Among them is the emergence of dual-mode sensor platforms, where a single sensor unit is capable of simultaneously measuring two different parameters [35,36]. The use of thin film layers allows for the placement of different sensing elements. In the case of cumulative buckling and magnetic cumulation, a chip simultaneously registers IR radiation (temperature changes) and detects THz pulses. Registering low-power magnetic dipole and IR radiation requires embedding a dual-mode sensor and a focusing lens in an antenna arrangement [37]. Recent progress in infrared-sensitive materials, strain engineering strategies, and device architectures is enabling flexible infrared photodetectors to maintain high performance under mechanical deformation, paving the way for scalable, robust, and application-ready devices [38].

The impact of the emergence of a wave, which exhibits properties akin to a combustion wave, on the degradation of thin S films subjected to pulses with sub-nanosecond risetime warrants further investigation. Films fabricated using the technique described in [21] are well-suited for this purpose. Particular attention should be paid to the method for incorporating artificial pinning centers into the films [39,40]. Such films, while maintaining high current density, can serve to mitigate the opposing interaction between the Meissner and Lorentz forces during propagation of the N zone. Furthermore, films that utilize precursor foams (polyurethanes with various densities, flexibilities, and skeleton types) were infiltrated with a green phase (Y-211) and thermally converted to Y-123 superconductor, could also yield favorable results under short pulse action. The opposition between Meissner and Lorentz forces is highly likely to be less pronounced in these foam-filled films, consequently increasing the durability of such S films during multiple S-N switching [41].

5. Conclusions

The reaction of the S state as the MCQS to its border integrity violation by a fast-rising magnetic field, induced by the flowing current, is virtually instantaneous. Therefore, the near-balanced counteraction of the Meissner and Lorentz forces leads to the bending instability of the S-N border at the film edges during pulse growth. This MHD bending instability leads to energy dissipation and the onset of N zone propagation. Due to various bifurcations, the bent S-N border constantly changes its shape in space and time as the N zone propagates. The appearance of droplet-shaped S-N border segments, the maintenance of which is energetically inefficient, forces the MCQS to reconnect the S currents creating a smooth border, separating small S areas. This could allow the creation of microscopic S areas procedure, although a drawback is their short lifetime. The propagation of the N zone during pulsed S-N switching is characterized by the flow of an ultrafast wave exhibiting combustion wave properties. During the propagation of the N zone the condition of the S–N border can be characterized as being constantly in a state of MHD Richtmyer–Meshkov

instability. Some prospective methods that leverage modern technologies for investigating the described phenomena are discussed.

Author Contributions: Conceptualization, O.K.; methodology, O.K.; validation, O.K. and L.A.; investigation, O.K.; data curation, O.K.; writing—original draft preparation, O.K.; writing—review and editing, O.K. and L.A.; visualization, O.K. and L.A. All authors have read and agreed to the published version of the manuscript.

Funding: This research received no external funding.

Institutional Review Board Statement: Not applicable.

Informed Consent Statement: Not applicable.

Data Availability Statement: Data sharing is not applicable to this article as no new data were created or analyzed in this study.

Conflicts of Interest: The authors declare no conflicts of interest.

References

1. Shepelev, A. The discovery of type II superconductors (Shubnikov phase). In *Superconductor*; Luiz, A.M., Ed.; InTech: Rijeka, Croatia, 2010; pp. 17–46. [CrossRef] [PubMed]
2. Kozhevnikov, V. Meissner effect: History of development and novel aspects. *J. Supercond. Nov. Magn.* **2021**, *34*, 1979–2009. [CrossRef]
3. Xiao-feng, P. Properties of macroscopic quantum effects and dynamic natures of electrons in superconductors. In *Superconductivity—Theory and Applications*; Luiz, A.M., Ed.; InTech: Rijeka, Croatia, 2011; pp. 173–212. [CrossRef] [PubMed]
4. Gallmann, L.; Lado, J.; Meijer, J.; Rossel, C. Quantum Science and Technologies. *Eur. News* **2025**, *56*, 14. [CrossRef]
5. Devoret, M.H.; Martinis, J.M.; Clarke, J. Measurements of macroscopic quantum tunneling out of the zero-voltage state of a current-biased Josephson junction. *Phys. Rev. Lett.* **1985**, *55*, 1908–1911. [CrossRef] [PubMed]
6. Sibanda, D.; Oyinbo, S.T.; Jen, T.-C.; Ibitoye, A.I. A mini review on thin film superconductors. *Processes* **2022**, *10*, 1184. [CrossRef]
7. Bolz, U.; Biehler, B.; Schmidt, D.; Runge, B.-U.; Leiderer, P. Dynamics of the dendritic flux instability in $YBa_2Cu_3O_{7-\delta}$. *Europhys. Lett.* **2003**, *64*, 517–523. [CrossRef]
8. Vestgården, J.; Mikheenko, P.; Galperin, Y.; Johansen, T. Nonlocal electrodynamics of normal and superconducting films. *New J. Phys.* **2013**, *15*, 093001. [CrossRef]
9. Kiprijanovič, O.; Ardaravičius, L.; Gradauskas, J.; Šimkevičius, Č.; Keršulis, S.; Ašmontas, S. Instability, magnetic flux trapping and cumulative effect during pulsed S-N switching of thin high quality YBaCuO films. *Supercond. Sci. Technol.* **2020**, *33*, 095013. [CrossRef]
10. Kiprijanovič, O.; Ardaravičius, L. Descriptive model of the transition from superconducting to normal state in thin high quality YBaCuO films by nanosecond electrical pulses. *Thin Solid Films* **2022**, *748*, 139159. [CrossRef]
11. Pearl, J. Current distribution in superconducting films carrying quantized fluxoids. *Appl. Phys. Lett.* **1964**, *5*, 65–66. [CrossRef]
12. Krasnov, V.M.; Katterwe, S.-O.; Rydh, A. Signatures of the electronic nature of pairing in high-*T*c superconductors obtained by non-equilibrium boson spectroscopy. *Nat. Commun.* **2013**, *4*, 2970. [CrossRef] [PubMed]
13. Belyaev, A.K.; Il'in, D.N.; Morozov, N.F. Dynamic approach to the Ishlinsky–Lavrent'ev problem. *Mech. Solids* **2013**, *48*, 504–508. [CrossRef]
14. Thoma, P.; Raasch, J.; Scheuring, A.; Hofherr, M.; Il'in, K.; Wünsch, S.; Semenov, A.; Hübers, H.-W.; Judin, V.; Müller, A.-S.; et al. Highly responsive YBaCuO thin film THz detectors with picosecond time resolution. *IEEE Trans. Appl. Supercond.* **2013**, *23*, 2400206. [CrossRef]
15. Dezardin, A.; Razanoelina, M.; Galiano, X.; Meautte, Y.; Tonouchi, M.; Kreisler, A. Semiconducting YBaCuO uncooled detectors: Feasibility of THz pyroelectric sensing. In *Proceedings of the 2018 43rd International Conference on Infrared, Millimeter, and Terahertz Waves (IRMMW-THz), Nagoya, Japan, 9–14 September 2018*; IEEE: Piscataway, NJ, USA, 2018; p. 8510161. [CrossRef]
16. Guo, S.; Li, C.; Wang, D.; Chen, W.; Gao, S.; Wu, G.; Xiong, J. Dual-band terahertz metamaterial sensor and its sensing capacity enhanced with a central-relief design. *Appl. Opt.* **2024**, *63*, 1962–1970. [CrossRef] [PubMed]
17. Ryzhii, V.; Ryzhii, M.; Ryabova, N.; Mitin, V.; Otsuji, T. Terahertz and infrared detectors based on graphene structures. *Infrared Phys. Technol.* **2011**, *54*, 302–305. [CrossRef]
18. Liu, J.; Li, X.; Jiang, R.; Yang, K.; Zhao, J.; Khan, S.A.; He, J.; Liu, P.; Zhu, J.; Zeng, B. Recent progress in the development of graphene detector for terahertz detection. *Sensors* **2021**, *21*, 4987. [CrossRef] [PubMed]

19. Tamura, K.; Tang, C.; Ogiura, D.; Suwa, K.; Fukidome, H.; Takida, Y.; Minamide, H.; Suemitsu, T.; Otsuji, T.; Satou, A. Fast and sensitive terahertz detection with a current-driven epitaxial-graphene asymmetric dual-grating-gate field-effect transistor structure. *APL Photonics* **2020**, *7*, 126101. [CrossRef]
20. Hongyi Ge, H.; Jia, K.; Jiang, Y.; Bu, Y.; Zhang, Y.; Zhang, Y.; Sun, Q. Dual-function terahertz metamaterial absorber based on microfluidic structures. *Opt. Express* **2025**, *33*, 3930–3949. [CrossRef] [PubMed]
21. Yadav, P.V.K.; Yadav, I.; Ajita, B.; Rajasekar, A.; Gupta, S.; Ashok Kumar Reggy, Y. Advancements of uncooled infrared microbolometer materials: A review. *Sens. Actuators A. Phys.* **2022**, *342*, 113611. [CrossRef]
22. Pęczkowski, P.; Zalecki, R.; Zachariasz, P.; Szostak, E.; Piętosa, J.; Turek, M.; Pyszniak, K.; Zając, M.; Czub, J.; Gondek, Ł. Deterioration of the 2G HTS tapes by the Ne^{+} ions irradiation (250 keV). *Appl. Sur. Sci.* **2023**, *636*, 157780. [CrossRef]
23. Davidson, P.A. *Introduction to Magnetohydrodynamics*, 2nd ed.; Cambridge University Press: Cambridge, UK, 2017; pp. 121–143.
24. Kiprijanovič, O.; Ardaravičius, L. Combustion wave properties of normal zone propagation induced by micro-sized magnetic cumulation in thin YBaCuO films. *Coatings* **2025**, *15*, 134. [CrossRef]
25. Strogatz, S.H. *Nonlinear Dynamics and Chaos*, 2nd ed.; CRC Press, Taylor & Frencis Group: Boca Raton, FL, USA, 2018; pp. 45–79.
26. Poston, T.; Stewart, I. *Catastrophe Theory and Its Applications*; Dover Publishing Inc.: Mineola, NY, USA, 1996; pp. 172–173, 307–320.
27. Hardy, G.H. Weierstrass's non-differentiable function. *Trans. Amer. Math. Soc.* **1916**, *17*, 301–325. [CrossRef]
28. David, C.; Lapidus, M. The Weierstrass Drift: A Toy SLE Brownian Model. HAL. 2025. Available online: https://hal.science/hal-05312686v1 (accessed on 12 March 2026).
29. Zhou, Y. Rayleigh–Taylor and Richtmyer–Meshkov instability induced flow, turbulence, and mixing. II. *Phys. Rep.* **2017**, *723*, 115–267.1–160. [CrossRef]
30. Brouillette, M. The Richtmyer-Meshkov instability. *Annu. Rev. Fluid Mech.* **2002**, *34*, 445–468. [CrossRef]
31. Wu, C.C.; Roberts, P.H. Richtmyer–Meshkov instability and the dynamics of the magnetosphere. *Geophys. Res. Lett.* **1999**, *26*, 655–658. [CrossRef]
32. Bezett, A.; Bychkov, V.; Lundh, E.; Kobyakov, D.; Marklund, M. Magnetic Richtmyer-Meshkov instability in a two-component Bose-Einstein condensate. *Phys. Rev. A* **2010**, *82*, 043608. [CrossRef]
33. Bond, D.; Wheatley, V.; Li, Y.; Samtaney, R.; Pullin, D.I. The magnetised Richtmyer–Meshkov instability in two-fluid plasmas. *J. Fluid Mech.* **2020**, *903*, A41. [CrossRef]
34. Zhang, S.-B.; Singh, S.; Torrilhon, M.; Zhang, H.-H.; Chen, Z.-H.; Zheng, C. Numerical investigation of Richtmyer–Meshkov instability in shock-driven light square bubble via magnetohydrodynamics. *Comput. Fluids* **2025**, *299*, 106698. [CrossRef]
35. Alda, J.; González, F.J. Fresnel zone antenna for dual-band detection at millimeter and infrared wavelengths. *Opt. Lett.* **2009**, *34*, 809–811. [CrossRef] [PubMed]
36. Gonzalo, R.; Iriarte, J.C.; Etayo, D.; Ederra, I. Dual band THz-IR detector for radio-astronomy applications. In *Proceedings of the 2015 International Symposium on Antennas and Propagation (ISAP), Hobart, TAS, Australia, 9–12 November 2015*; IEEE: Piscataway, NJ, USA, 2015; p. 7447314.
37. Torres-García, A.E.; Orazbayev, B.; Gonzalo, R.; Ederra, I. Dual-band integrated detector for THz and IR based on quasi-spiral antenna coupled to schottky diode. In *Proceedings of the 2016 IEEE International Symposium on Antennas and Propagation (APSURSI), Fajardo, PR, USA, 26 June–1 July 2016*; IEEE: Piscataway, NJ, USA, 2016; pp. 1193–1194. [CrossRef]
38. Balendhran, S.; Mousavi Khaleghi, S.S.; Fan, D.; Crozier, K.B. Flexible infrared photodetectors: Building blocks and prospects. *npj Nanophoton.* **2026**, *3*, 45. [CrossRef]
39. Crisan, A.; Badica, P.; Fujiwara, S.; Nie, J.-C.; Sundaresan, A.; Iyo, A.; Tanaka, Y. Nanodots-induced pinning centers in thin films: Effects on critical current density, activation energy and flux jump rate. *IEEE Trans. Appl. Supercond.* **2003**, *13*, 3726–3729. [CrossRef]
40. Zhang, J.; Wu, H.; Zhao, G.; Hun, L.; Zhang, J. Progress in the study of vortex pinning centers in high-temperature superconducting films. *Nanomaterials* **2022**, *12*, 4000. [CrossRef] [PubMed]
41. Pęczkowski, P.; Zachariasz, P.; Zalecki, R.; Piętosa, J.; Michalik, J.; Jastrzębski, C.; Ziętala, M.; Zając, M.; Gondek, Ł. Influence of polyurethane skeleton on structural and superconducting properties of Y-123 foams. *J. Eur. Ceram. Soc.* **2024**, *44*, 5722–5730. [CrossRef]

Disclaimer/Publisher's Note: The statements, opinions and data contained in all publications are solely those of the individual author(s) and contributor(s) and not of MDPI and/or the editor(s). MDPI and/or the editor(s) disclaim responsibility for any injury to people or property resulting from any ideas, methods, instructions or products referred to in the content.